Check for updates

Daniel Niehaus[1,*]
Anastasios Lyberis[2]
Selma Iraqi Houssaini[1]
Zeynep Perçin[2]
Gregor Liebsch[3]
Paul Bubenheim[2]
Marko Hoffmann[1]
Andreas Liese[2]
Michael Schlüter[1]

High-Pressure Reactor Technology for Aerated Biotransformations

Utilizing pressure as a process parameter can make biotechnological processes more efficient and attractive compared to established ones. This paper presents a high-pressure reactor setup for enzymatically catalyzed gas–liquid reactions, which can be operated up to 15.0 MPa. The reactor is equipped with optical measurement technology for inline and in situ monitoring of the oxygen concentration under high-pressure conditions. The setup is characterized by assessing the influence of the process parameter pressure on the conversion of the glucose oxidation to D-glucono-δ-lactone by immobilized glucose oxidase. The study demonstrates that the increased oxygen availability due to higher solubility reduces the reaction time in a batch reactor from 270 to 90 min.

Keywords: Aerated biotechnological reactor, Glucose oxidase, High pressure, Optical oxygen measurement, Process intensification

Received: January 26, 2024; *revised:* June 27, 2024; *accepted:* November 05, 2024

DOI: 10.1002/ceat.202400043

This is an open access article under the terms of the Creative Commons Attribution License, which permits use, distribution and reproduction in any medium, provided the original work is properly cited.

1 Introduction

In response to growing environmental consciousness, biotechnology has gained significance in fine chemical production. Leveraging pressure as a process parameter can further advance this trend. Although the impact of temperature on enzyme stability and catalytic activity is well known [1, 2], recent research highlights the potential impact of pressure to intensify processes [3, 4], influencing enzyme stability, activity [5, 6], and selectivity [7]. Despite pressure being used for enzyme deactivation in food industry, its process-intensifying potential faces underutilization due to challenges. These include the need for detailed research on pressure effects and limited technology for online monitoring and effective control under pressure.

This study introduces a reactor concept addressing these challenges, facilitating in-depth investigation of enzyme-catalyzed reactions under high pressure. The development of this reactor system involves the incorporation of optical sensors for monitoring the oxygen concentration and the pH of the reaction medium. The functionality of this reactor and measurement technique is demonstrated through the investigation of the oxidation reaction of D-glucose to D-glucono-δ-lactone using immobilized glucose oxidase.

1.1 Enzymatic Reactions under Pressure

Pressure induces changes in enzyme activity, stability, and selectivity, typically attributed to alterations in enzyme conformation, reaction mechanism, or the physical properties of the substrate. Scientific exploration of the impact of pressure on enzyme structure dates back to Bridgman in 1914 [8], studying egg coagulation under pressure. Although high pressure in biotechnology is mostly employed in the food industry for enzyme inactivation to increase the shelf life of food [9, 10], conformational changes induced by pressure also affect catalytic activity by altering the shape and function of the active site. Furthermore, pressure can affect the reaction equilibrium, which is characterized by negative values of activation volumes ($\Delta V^{\neq}$). Pressure also enhances the thermal stability of certain enzymes [11].

Numerous factors acting on distinct parts of enzyme structure make predicting pressure effects challenging. Ongoing research aims to identify molecular and process-level factors influenced both negatively and positively by pressure [3, 4, 12]. Additionally, pressure can influence the enantioselectivity and various substrate and solvent properties, including pH, viscosity, and density, as well as gas solubility being of key interest in gas-liquid

[1]Daniel Niehaus https://orcid.org/0000-0001-7217-7583 (Daniel.niehaus@tuhh.de), Selma Iraqi Houssaini https://orcid.org/0009-0008-9856-1776, Marko Hoffmann, Michael Schlüter https://orcid.org/0000-0001-5969-2150
Institute of Multiphase Flows, Hamburg University of Technology, Eißendorfer Str. 38, 21073 Hamburg, Germany.
[2]Anastasios Lyberis https://orcid.org/0000-0003-4960-2929, Zeynep Perçin https://orcid.org/0000-0002-1291-7380, Paul Bubenheim https://orcid.org/0000-0001-6954-4274, Andreas Liese https://orcid.org/0000-0002-4867-9935
Institute of Technical Biocatalysis, Hamburg University of Technology, Denickestr. 15, 21073 Hamburg, Germany.
[3]Gregor Liebsch https://orcid.org/0009-0006-5473-4466
PreSens Precision Sensing GmbH, Am Biopark 11, 93053 Regensburg, Germany.

 © 2024 The Author(s). Chemical Engineering & Technology published by Wiley-VCH GmbH

reactions [13, 14]. As Chapman [15] points out in particular, oxidases are often subject to limitations due to the available dissolved oxygen; therefore, glucose oxidase is investigated as a model reaction system. An approach to describe gas solubility is Henry's law. It describes gas solubility for systems in equilibrium as a function of partial pressure and temperature according to the following equation:

$$c_i = K_H\,(T)\,p_i \tag{1}$$

Henry's law links the maximum solubility of a gas c_i in a liquid to the gas's partial pressure p_i, incorporating a temperature-dependent, substance-specific solubility coefficient K_H. Applicable at low pressures, it assumes no interaction between the dissolved gas and solvent.

1.2 Mass Transfer in Aerated Reactors

The mass transfer of oxygen can be calculated according to the two-film theory of Lewis and Whitman [16]:

$$\frac{\mathrm{d}c_{O_2}}{\mathrm{d}t} = k_l a \times \left(c^*_{O_2} - c^{\infty}_{O_2}(t)\right) \tag{2}$$

The theory describes the change in oxygen concentration using the mass transfer coefficient k_l, the difference between the bulk concentration $c^{\infty}_{O_2}$ and the saturation concentration $c^*_{O_2}$ as well as the volume-specific mass transfer area a. The area for mass transfer can be calculated via the gas hold-up ε_G and the Sauter mean diameter d_{32} of the gas bubbles according to

$$a = \frac{6\varepsilon_g}{d_{32}} \tag{3}$$

Eqs. 2 and 3 reveal two key factors driving increased mass transfer under pressure. First, the maximum solubility of oxygen $c^*_{O_2}$. An increase in pressure leads to an increase in maximum oxygen solubility. Second, according to Wilkinson [17], a reduction in the bubble diameter d_{32} and an increase in the gas hold-up ε_g can be observed, and thus, a significant increase in the mass transfer area can be achieved.

2 Materials and Methods

The reactor concept in this study spatially separates aeration and enzymatic reaction, countering the negative impacts of direct aeration on enzyme stability [18]. Previous studies highlight shear forces [19] and enzyme–gas–liquid interaction [20, 21] as key factors causing denaturation in aerated systems. Achieving spatial separation addresses both issues.

The aeration unit and the bioreactor with immobilized enzymes are interconnected, forming a circulation loop. Via the periphery, a liquid flow with constant temperature, pH, and operating pressure can be established during continuous aeration. Optical oxygen sensors (SP-PST3, PreSens Precision Sensing GmbH, Regensburg, Germany) in the circuit monitor oxygen concentration inline and in situ. In addition, samples are withdrawn from the system and analyzed offline using high-performance liquid chromatography (HPLC). All data from sensors are recorded via the process control system WinErs (Ingenieurbüro Dr.-Ing. Schoop GmbH, Hamburg, Germany). The pipe and instrumentation flow diagram of the reactor is shown in Fig. 1.

2.1 Aeration Unit

The aeration unit saturates the liquid with oxygen for the enzymatic reaction. The aeration unit is a bubble column ($V_{bc} = 38$ mL) operated in counter-current flow (Fig. 2a). The unit is equipped with an observation window for optical examinations under pressure. The liquid enters from the top of the cell and flows out at the bottom. The gaseous phase, consisting of technical compressed air (79 % N_2, 21 % O_2, oil-free), is injected at the bottom of the aeration unit via a capillary ($d_c = 1.9$ mm). This non-moving-parts design is preferred for high-pressure applications and scalable operations [22].

The gas inlet flow is regulated by a mass flow meter (EL-FLOW F111B, Bronkhorst, Kamen, Germany), providing a standard volume flow rate of 3.5–85.0 mL s^{-1}. The headspace of the bubble column is filled with gas, and a back pressure regulator (Pressure Control Solutions, Veenendaal, The Netherlands) allows a precise pressure adjustment of the headspace within the range of 0.2–15.0 $\pm$ 0.01 MPa, regulating the entire system's pressure. To characterize the aeration unit, optical analysis determines the bubble size distribution. Using these data, the Sauter mean diameter and gas hold-up are calculated, considering operating pressure and superficial gas velocity u_g. The velocity is derived from the injected gas volume flow rate $\dot{V}_g$ and the cross-sectional area of the bubble column A_{bc}, as follows:

$$u_g = \frac{\dot{V}_g}{A_{bc}} \tag{4}$$

2.2 Bioreactor

The enzymes are immobilized within a separate cylindrical bioreactor (Fig. 2b) with an internal diameter of 41 mm, offering a 150 mL total volume. A gear pump (GA 180, Axflow GmbH, Düsseldorf, Germany) ensures a controlled flow rate of oxygen-saturated liquid phase (between 0.15 and 1.5 mL s^{-1}) through the bioreactor. Positioned at the bottom of the aeration cell, the pump draws in the liquid phase and circulates it through the bioreactor, returning it to the top of the aeration cell. The flow is measured by a coriolis mass flow meter (CORI-FLOW, M14, Bronkhorst, Kamen, Germany) and maintained constant through a control loop adjusting the pump's rotational speed. For the experiments, the reactor is filled with glucose oxidase immobilized on epoxy-functionalized porous polymethacrylate particles (ReliZyme^{TM} HFA-403, Resindion). Retained within the bioreactor by sinter stone filters at both ends, these enzyme-immobilized particles facilitate the experimental procedure.

2.3 Optical Measurement Technique

The setup employs fluorescence-based optical sensors for real-time, in situ monitoring of dissolved oxygen concentration and

 © 2024 The Author(s). Chemical Engineering & Technology published by Wiley-VCH GmbH

15214125, 0, Downloaded from https://onlinelibrary.wiley.com/doi/10.1002/ceat.202400043 by Technische Universität Hamburg Universitätsbibliothek, Wiley Online Library on [10/12/2024]. See the Terms and Conditions (https://onlinelibrary.wiley.com/terms-and-conditions) on Wiley Online Library for rules of use; OA articles are governed by the applicable Creative Commons License

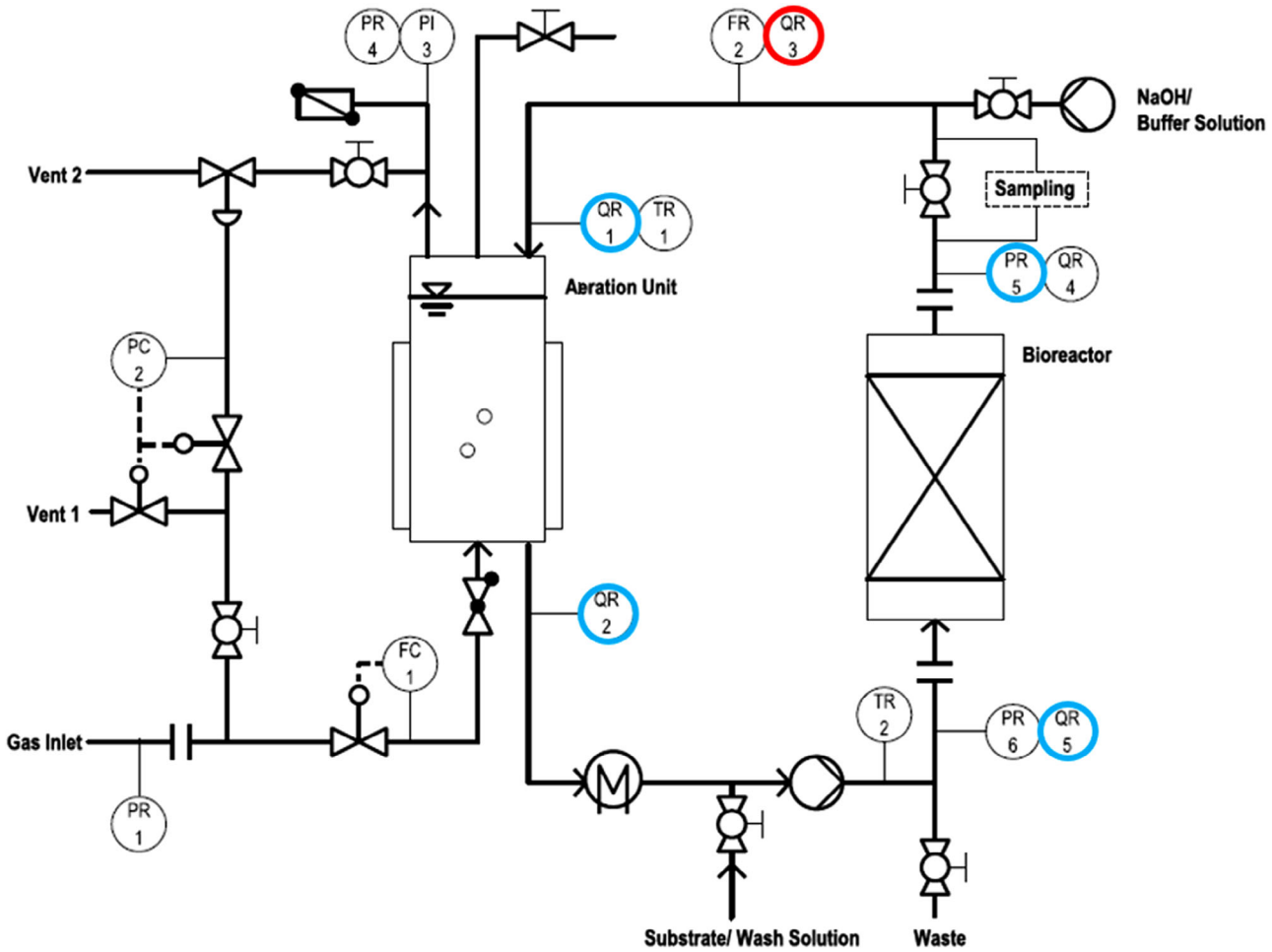

Figure 1. Tube and instrumentation flow diagram of the reactor setup. The optical oxygen sensors integrated within the setup are indicated by the blue markers, and the pH probe used is indicated by the red marker.

pH (SP-PST3 and SP HP5, PreSens Precision Sensing GmbH, Regensburg, Germany). These sensors utilize dynamic fluorescence quenching, involving the interaction of a metalloporphyrin in a polymer with a quencher (e.g., oxygen). pH determination uses dual-lifetime referencing, measuring intensity deviation from a reference fluorophore [23]. Oxygen measurement relies on frequency-domain principles, capturing the decay time–dependent phase shift φ between the excitation signal and fluorescence decay. This is quantitatively correlated to the oxygen concentration through the Stern–Volmer relationship [24]. Eq. 5 defines the Stern–Volmer relationship, where the ratio of fluorescence intensity in the unquenched state I_0 to the quenched state I is described by the Stern–Volmer constant K_{SV} and the concentration of the quencher (Q). The Stern–Volmer constant can be expressed as the product of the bimolecular quenching constant k_Q and the lifetime of fluorescence in the unquenched state τ_0. Graphical representation of the Stern–Volmer equation is shown in Fig. 3:

$$\frac{I_0}{I} = 1 + k_Q \tau_0 [Q] = 1 + K_{SV} [Q] \quad (5)$$

The optical dissolved oxygen sensors used here offer advantages over established methods like Winkler titration or electrodes. Titration would require direct substrate access and consistent pressure conditions to prevent oxygen outgassing. Electrodes also possess certain characteristics that hinder their suitability for high-pressure environments. In contrast to optodes, they need a cable duct through the outer shell of the high-pressure reactor. Additionally, the electrode introduces an external potential and alters the dissolved oxygen during measurement. Equally important is the boundary layer at the electrode, which significantly impacts the precision and speed of the measurement. This necessitates calibration based on the prevailing flow conditions. If flow conditions vary over time, it affects the measurement behavior of the electrode [25]. The parameter τ_0 represents the decay time, an intrinsic property of the fluorescent dye, and is determined in our study by sinusoidal modulation of the excitation light and measurement of the phase angle φ, which corresponds to the time delay of the fluorescence waves relative to the excitation light waves. τ_0 is free from intensity-dependent disturbances and can thus be directly utilized as a raw measurement result.

 © 2024 The Author(s). Chemical Engineering & Technology published by Wiley-VCH GmbH

15214125, 0, Downloaded from https://onlinelibrary.wiley.com/doi/10.1002/ceat.202400043 by Technische Universität Hamburg Universitätsbibliothek, Wiley Online Library on [10/12/2024]. See the Terms and Conditions (https://onlinelibrary.wiley.com/terms-and-conditions) on Wiley Online Library for rules of use; OA articles are governed by the applicable Creative Commons License

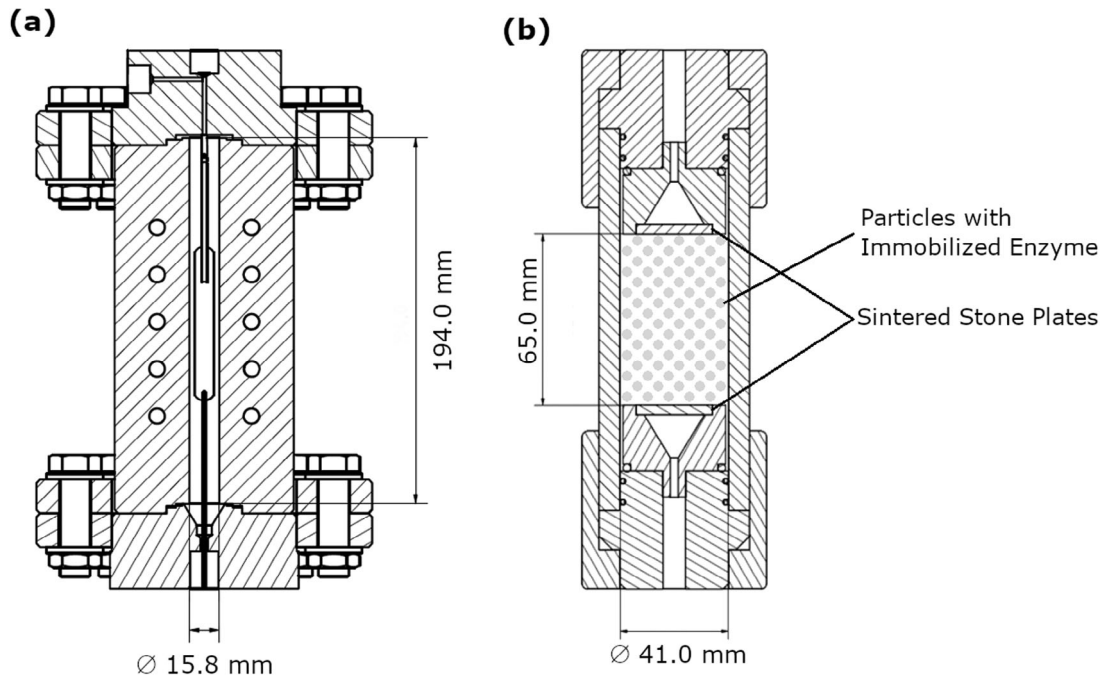

Figure 2. Sectional view (a) through the viewing cell and (b) the bioreactor with particle retention.

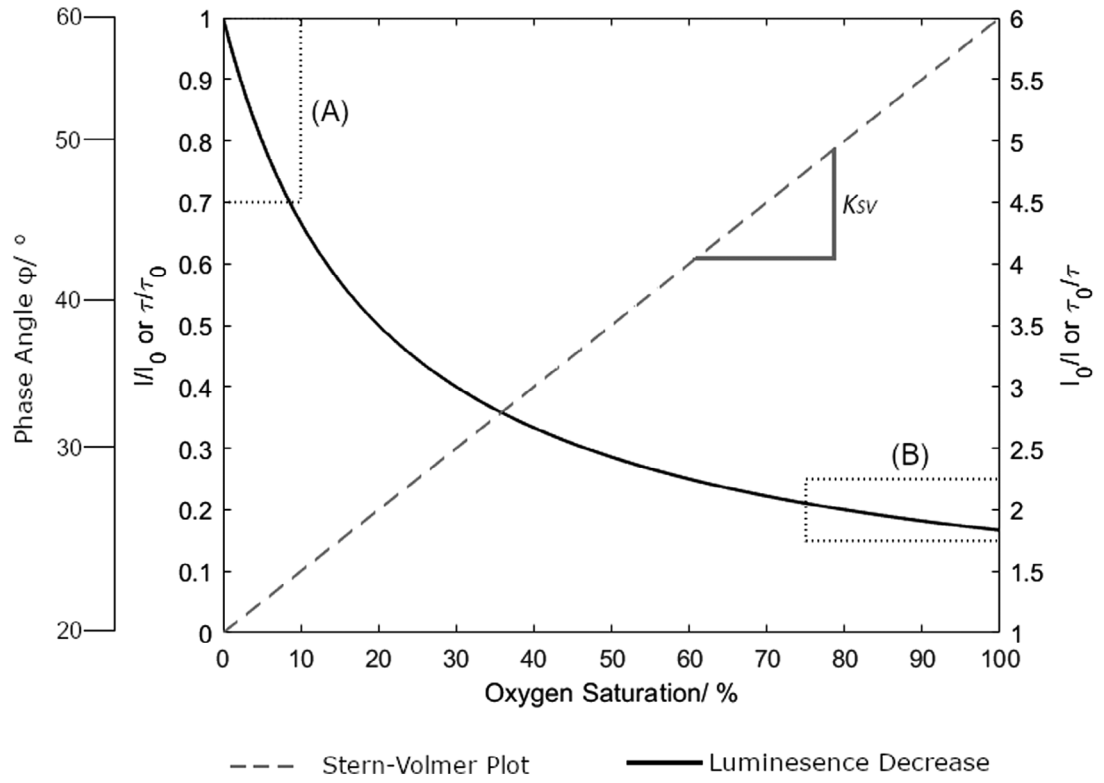

Figure 3. Quenching behavior of a fluorophore as a function of oxygen saturation (atmospheric conditions) and its linearization by the Stern–Volmer equation.

 © 2024 The Author(s). Chemical Engineering & Technology published by Wiley-VCH GmbH

15214125, 0, Downloaded from https://onlinelibrary.wiley.com/doi/10.1002/ceat.202400043 by Technische Universität Hamburg Universitätsbibliothek, Wiley Online Library on [10/12/2024]. See the Terms and Conditions (https://onlinelibrary.wiley.com/terms-and-conditions) on Wiley Online Library for rules of use; OA articles are governed by the applicable Creative Commons License

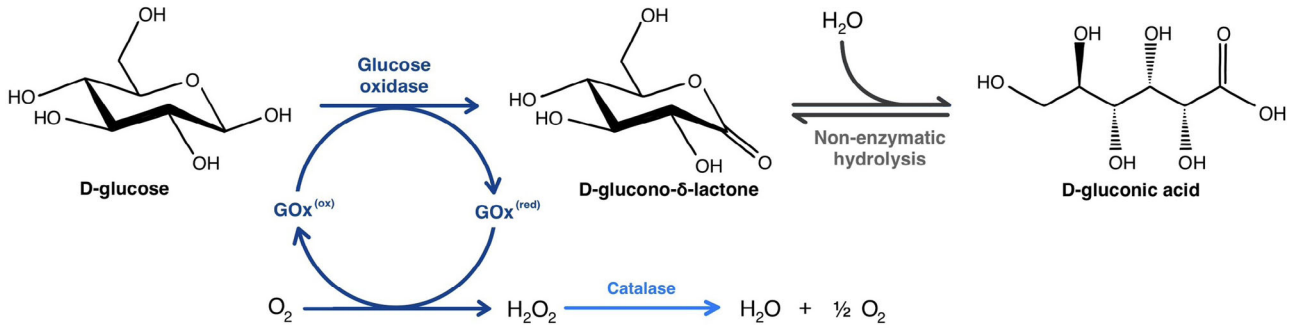

Figure 4. Reaction scheme of the chemoenzymatic synthesis of d-gluconic acid from d-glucose and molecular O_2 by *glucose oxidase* and H_2O_2 depletion by *catalase*.

Concerning optical oxygen measurements under pressure, past studies have shown the Stern–Volmer equation having a non-linear behavior under pressure [26, 27]. Optodes have been utilized for high-pressure oxygen measurements in deep-sea conditions [28, 29], where low-oxygen concentrations are encountered. Although optodes demonstrate commendable dynamic response in these conditions (Fig. 3a), this study focuses on measurements well above atmospheric saturation, where optodes show modest dynamic performance (Fig. 3b). A crucial point of this study is to evaluate whether optical oxygen measurements can accurately monitor the enzymatic reaction's progress under these conditions.

2.4 Hydrodynamic Characterization

The hydrodynamic parameters crucial for the mass transfer area, the mean Sauter diameter d_{32} and the gas hold-up ε_g, were assessed by optical investigation of the bubble size distribution. To assess the distribution, the setup was filled with deionized water and aerated with technical compressed air (oil-free, Westfalen AG, Münster, Germany) at different pressures and volume flow rates. Utilizing a Nikon D 90 digital camera and a Macro Nikkor lens with a 105 mm focal length, 300 images (n_{im}) were captured at each measuring point with an 8 Hz acquisition frequency. The used lens provided a spatial resolution of 9.12 µm pix^{-1}. To enhance contrast at the bubble interface, a high-power LED panel was positioned at the back of the viewing cell.

The images were analyzed, and the bubble size distribution was determined using Smart Online Particle Analysis Technology's (SOPAT's) evaluation software (v2.1.17.1623), featuring a trainable algorithm for detecting particles and bubbles. This enables the detection and determination of the bubble size distribution in the images. Based on the bubble size distribution, the Sauter mean diameter d_{32} can be calculated according to

$$d_{32} = \frac{\sum_i n_i d_i^3}{\sum_i n_i d_i^2} \tag{6}$$

With a visible cell depth of less than 1 cm and nearly spherical bubbles under increased pressure, the gas hold-up ε_g is determined. This involves multiplying the number of bubbles by their respective volumes based on the bubble diameter (d_i). This calculation, following Eq. 7 across the entire size spectrum, yields the gas volume, which is then related to the designated liquid volume (V_{bc}):

$$\varepsilon_g = \frac{\sum_i n_i \times \left(\frac{\pi}{6} d_i^3\right)}{V_{bc} n_{im}} \tag{7}$$

2.5 Model Reaction System

To investigate the behavior of the enzymatic reaction under pressure, the oxidation of glucose to D-gluconic acid catalyzed by glucose oxidase, as depicted in Fig. 4, is chosen as a model reaction. The reaction scheme includes the enzymatic oxidation of glucose by molecular oxygen to D-glucono-δ-lactone as well as the subsequent non-enzymatic hydrolysis of the lactone to D-gluconic acid. Furthermore, catalase is required in the system to avoid H_2O_2 accumulation. Under atmospheric conditions, mass transfer limitations dominate the reaction system due to low oxygen solubility in aqueous media. Increased pressure enhances oxygen solubility, having the potential to enhance the activity of glucose oxidase [18, 30, 31].

2.5.1 Enzyme Immobilization

Glucose oxidase from *Aspergillus niger* was covalently immobilized on porous polymethacrylate carrier particles with an epoxy-functionalized surface (ReliZyme™ HFA-403 by Resindion). Following the method outlined by Perçin et al. [32], this involves a covalent multipoint immobilization, creating chemical bonds between amino-groups of the enzyme and exposed epoxy-groups on the carrier particle surface. A solution of glucose oxidase in sodium acetate buffer (100 mM, pH 5.4) was prepared, and 10 g of dry carrier particles were added, reaching a final enzyme loading of 2.9 mg of enzyme per g of carrier particles.

2.6 Process Control

To measure enzyme activity, immobilized enzymes were inserted into the bioreactor. Before the experiment, the setup was evacuated and charged with the substrate, which was a 0.1 M glucose solution in sodium acetate buffer (100 mM). To start up the operation and to reach the desired point of operation, the substrate was circulated at 1.33 mL s^{-1} while being flushed with nitrogen.

 © 2024 The Author(s). Chemical Engineering & Technology published by Wiley-VCH GmbH

15214125, 0, Downloaded from https://onlinelibrary.wiley.com/doi/10.1002/ceat.202400043 by Technische Universität Hamburg Universitätsbibliothek, Wiley Online Library on [10/12/2024]. See the Terms and Conditions (https://onlinelibrary.wiley.com/terms-and-conditions) on Wiley Online Library for rules of use; OA articles are governed by the applicable Creative Commons License

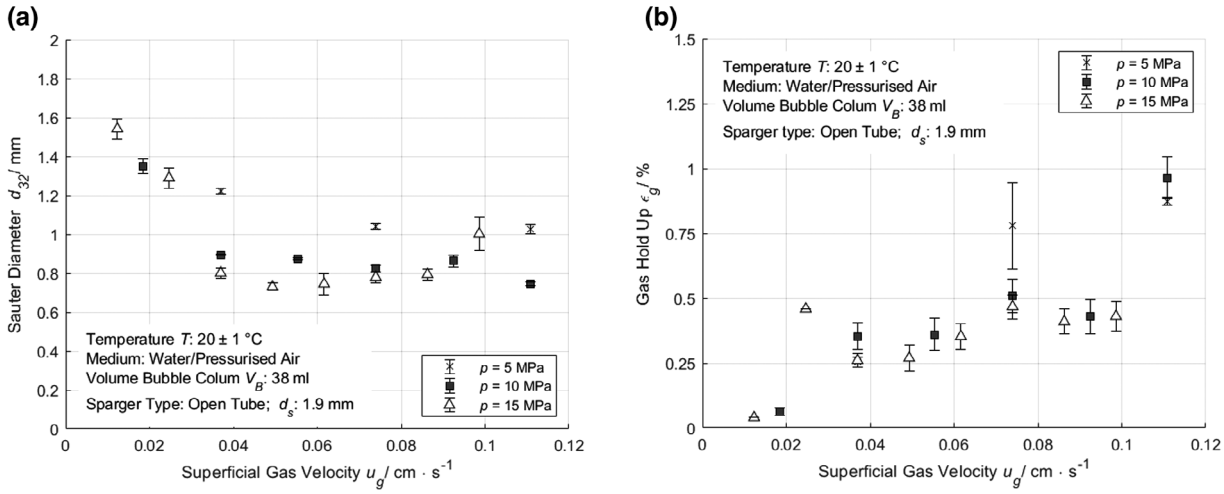

Figure 5. Sauter mean diameter (a) and gas hold-up (b) as a function of the superficial gas velocity and the operating pressures.

The liquid medium was heated to 35 °C, the temperature optimum for glucose oxidase. The backpressure regulator was employed to set the desired pressure (0.3–15.0 MPa). When the chosen operating pressure and temperature were achieved, the gas supply shifted from nitrogen to compressed air, with a constant gas flow rate. During the experiment, the temperature was kept at 35 °C and the pH-value at 5.4. These values have proven to be the optimal operating conditions for the glucose oxidase used, ensuring high activity [33–35].

To maintain pH when buffer capacity is surpassed, a pH sensor and syringe pump acted as an autotitrator to shift the equilibrium from D-glucono-δ-lactone to the side of the gluconic acid. A 2N NaOH solution is dosed at the bioreactor outlet. The Dosage of the solution is monitored automatically and continuously via a PI controller integrated into the process control system. Recirculation via the aeration cell ensures proper mixing and dilution of the concentrated base, preventing enzyme deactivation from pH fluctuations.

2.7 Analytics and Data Evaluation

The setup features four optical oxygen sensors, QR 1–2 and QR 4–5, monitoring the gaseous reactant, a primary limiting factor. By comparing sensors QR 4 and QR 5 at the bioreactor inlet and outlet, oxygen consumption by the enzyme is tracked. When the reaction stops, e.g., by complete substrate consumption or after reaching chemical equilibrium, the oxygen concentration at both measurement points equalizes.

To validate sensor data, liquid samples are drawn every 2.5 min during the reaction using a bypass and an HPLC valve (6 Port 2 Pos, VICI Valco Instruments, Houston, USA). The valve has a sampling loop with a volume of 250 µL. The sample volume is displaced with sodium acetate buffer (100 mM, pH 5.4) via an additional syringe pump and filled into a vial. The samples are analyzed by HPLC using a NUCLEODUR® column (3 µm, 110 Å, RP C18, Macherey-Nagel, Düren, DE) to track the formation of D-gluconic acid. The analysis was performed at 25 °C using an aqueous mobile phase that contained 20 mM phosphoric acid (pH 2.0). The flow rate was 1.0 mL min^{-1}, and the retention time of gluconic acid was 0.8 min, detected by a DAD detector at 210 nm. The samples were reinjected after 10 and 24 h from the initial injection without any noticeable change in the obtained signals. This was an indicator that no measurable enzyme leaching occurred during the reaction. The gluconic acid progress curve was used to calculate the initial reaction rate, determining the activity of the immobilized enzyme.

3 Hydrodynamic Characterization

Oxygen availability is pivotal for the characterization of the enzymatic reaction under pressure. The behavior of the open tube sparger is analyzed at varying pressure (0.3–15.0 MPa) and superficial gas velocity (0–0.12 cm s^{-1}). Eq. 2 highlights the crucial role of mass transfer area a, determined by the Sauter mean diameter and gas hold-up (Eq. 3). Fig. 5 illustrates how the Sauter mean diameter and gas hold-up vary with pressure and superficial gas velocity.

The Sauter diameter ranges from 1.2 to 1.6 mm at superficial gas velocities below 0.02 cm s^{-1} for all considered pressures. With increasing superficial gas velocity, the diameter significantly decreases to a certain level. This level is dependent on the operating pressure—1 mm at 5.0 MPa, 0.85 mm at 10.0 MPa, and 0.75 mm at 15.0 MPa. The increase between 10.0 and 15.0 MPa is notably smaller than between 5.0 and 10.0 MPa.

This trend is mirrored in the gas hold-up, determined by Eq. 7. The hold-up increases across all pressure levels with rising superficial gas velocity. At 0.02 cm s^{-1}, a clear jump in the hold-up is observed. As Fig. 6 shows, this change results from a shift in the bubble regime. Single-ascending bubbles dominate at low velocities (Fig. 6a), whereas jet gassing becomes predominant at higher velocities (Fig. 6b). Fig. 6c displays bubble detection by the SOPAT algorithm marked in green, recognizing almost all bubbles; however, smaller bubbles may go unnoticed, as the resolution limit for bubbles is approximately 0.1 mm. Tests at higher superficial velocities reveal smaller secondary bubbles, limiting optical evaluation techniques efficacy.

 © 2024 The Author(s). Chemical Engineering & Technology published by Wiley-VCH GmbH

15214125, 0, Downloaded from https://onlinelibrary.wiley.com/doi/10.1002/ceat.202400043 by Technische Universität Hamburg Universitätsbibliothek, Wiley Online Library on [10/12/2024]. See the Terms and Conditions (https://onlinelibrary.wiley.com/terms-and-conditions) on Wiley Online Library for rules of use; OA articles are governed by the applicable Creative Commons License

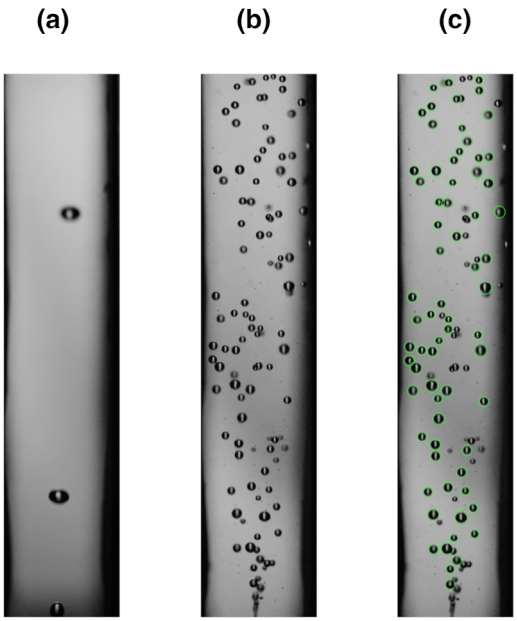

Figure 6. Bubble regime in the aeration cell at 15.0 MPa and a superficial gas velocity of (a) 0.01 cm s^{-1}; (b) 0.025 cm s^{-1}; (c) image b analyzed by SOPAT with detected bubbles being color-coded. Reaction conditions: $T = 20$ °C, deionized water/technical compressed air.

Eq. 3 calculates the volume-specific mass transfer area (a) using gas hold-up and the Sauter mean diameter. At superficial gas velocities below 0.02 cm s^{-1}, the graph shows consistently low interfacial areas, remaining below 10 m^2 m^{-3} across different pressures. This is attributed to single-bubble rise and larger Sauter mean diameter. Above 0.04 cm s^{-1}, within the range of 10.0–15.0 MPa, a relatively stable interfacial area between 20 and 30 m^2 m^{-3} is achieved (Fig 7).

To optimize mass transfer, a superficial gas velocity exceeding 0.02 cm s^{-1} is recommended. Below this value, only individual bubbles rise, especially evident at lower pressures. Increasing pressure slightly decreases the Sauter mean diameter, influenced by changes in bubble coalescence and disintegration behavior. Elevated gas density intensifies instabilities, resulting in more bubble ruptures and reduced coalescence, producing a narrower bubble size distribution [36]. Our findings align with studies indicating a pressure plateau, beyond which further increase minimally impacts the bubble diameter [37, 38]. This plateau is evident in our data, with marginal differences in bubble size between 10.0 and 15.0 MPa.

4 Study of Enzymatic Reaction under Pressure

The setup and optical measurement technique are validated using immobilized glucose oxidase from *A. niger* (≤8 kU of free enzyme immobilized on 10 g of carrier particles). Glucose oxidase was acquired as a lyophilized powder by Sigma-Aldrich. Glucose oxidation was tested across the entire pressure range from 0.3 to 15.0 MPa under constant experimental conditions. Parameters, including temperature at 35 °C, standard volume flow of 5 mL s^{-1}, and a pH of 5.4, were kept constant throughout the experiments. Catalase from *Corynebacterium glutamicum* (≤1 kU) was added in its free form to the reaction medium in the form of an enzyme solution—as acquired by Sigma-Aldrich—in a sufficient amount so as to prevent H_2O_2 accumulation. Analytical-grade chemicals were sourced from Roth (Karlsruhe, Germany) or Sigma-Aldrich (Vienna, Austria).

The monitoring of the oxygen concentration during the experiment was of particular interest due to the limiting character of the dissolved oxygen. Fig. 8 shows the course of the phase angle, the primary measured variable, during a test run at an operating pressure of 5.0 MPa. The data at the inlet (black) and the outlet (grey) of the bioreactor are shown here.

As expected, the initial phase angle is at 58°, which indicates a low oxygen concentration in the solution. Aeration initiates oxygen saturation, reflected in a decreasing phase angle at the bioreactor inlet. After the start-up phase, a nearly constant phase angle ($\varphi_{In,Stat}$) is observed. Oxygen concentration and phase angle are inversely related. Since the oxygen saturation is increased with pressure, the measured phase angles range from 14° at 0.3 MPa, 10° at 10.0 MPa, to around 9° at 15.0 MPa. Exact determination of absolute oxygen concentration is challenging. Within the range of 58°–25° (white background) in Fig. 8, the linear Stern–Volmer equation (Eq. 4) reliably approximates the relationship between phase angle and oxygen concentration. Calibration experiments have demonstrated that the oxygen concentration in the liquid can be measured until a detection limit of minimum 4° phase angle (light gray background color), corresponding to a solubility of about 250 mg L^{-1} O_2 (7.81 mM). As

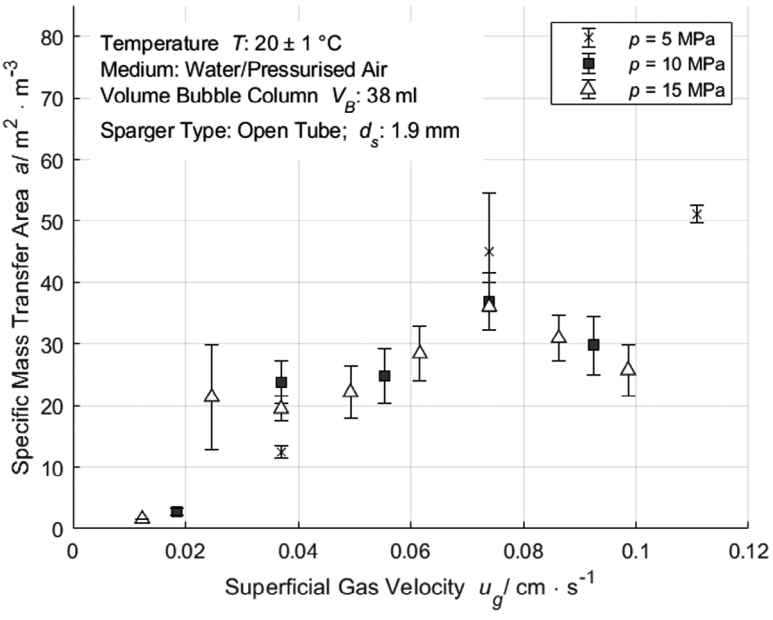

Figure 7. Mass transfer area as a function of the superficial gas velocity and the operating pressure.

 © 2024 The Author(s). Chemical Engineering & Technology published by Wiley-VCH GmbH

15214125, 0, Downloaded from https://onlinelibrary.wiley.com/doi/10.1002/ceat.202400043 by Technische Universität Hamburg Universitätsbibliothek, Wiley Online Library on [10/12/2024]. See the Terms and Conditions (https://onlinelibrary.wiley.com/terms-and-conditions) on Wiley Online Library for rules of use; OA articles are governed by the applicable Creative Commons License

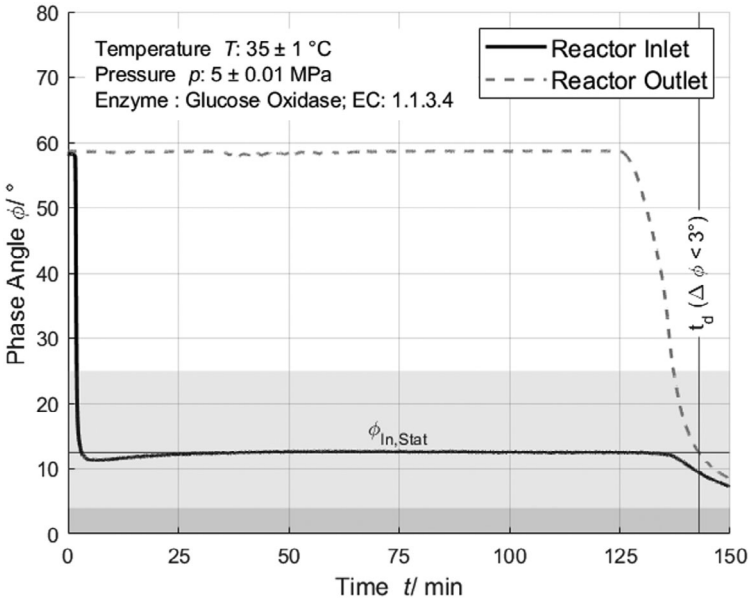

Figure 8. Time course of the phase angle before (gray dashed line) and after (black solid line) the bioreactor during an experimental run at 5.0 MPa. Conversion of glucose over time at 5.0 MPa. Reaction Conditions: $T = 35$ °C, filling volume: 170 mL, 100 mM sodium acetate buffer at pH 5.4, enzyme loading of glucose oxidase: 2.9 $mg_e\ g_{carrier}^{-1}$, $\dot{V}_l$: 80 mL min^{-1}, $\dot{V}_g$: 300 $mL_N\ min^{-1}$.

shown in Fig. 3, the linearity and sensitivity of the measurement technology decrease with increasing oxygen concentration. Below a phase angle of 4°, the sensitivity diminishes to a level that falls below the measurement error of the hardware used. Beyond this point, further differentiation becomes unfeasible (dark gray background).

The disparity between measurements at the inlet and outlet of the bioreactor indicates oxygen consumption facilitated by glucose oxidase. Furthermore, a constant phase angle of 58° at the reactor outlet suggests that a significant portion of the oxygen is consumed after passing through the bioreactor. Toward the end of the experiment, convergence of the sensor readings at the inlet and outlet of the bioreactor can be observed. This implies a diminishing oxygen consumption across the bioreactor until no further consumption is detected. Consequently, a criterion of less than 3° difference between the two sensors was applied to stop the experiment and determine the total reaction time (t_d). Fig. 9 illustrates the relationship between pressure and reaction time.

The graph shows a decrease in the experimental duration (t_d) with increasing pressure. The most significant reduction occurs from 0.3 to 2.5 MPa, decreasing from approximately 230 to under 150 min. Between 5.0 and 15.0 MPa, the reaction time further decreases to just under 80 min. This shows that a higher dissolved oxygen concentration at elevated pressure accelerates the reaction. To validate this conclusion, liquid samples were analyzed by HPLC. Results are shown in Fig. 10.

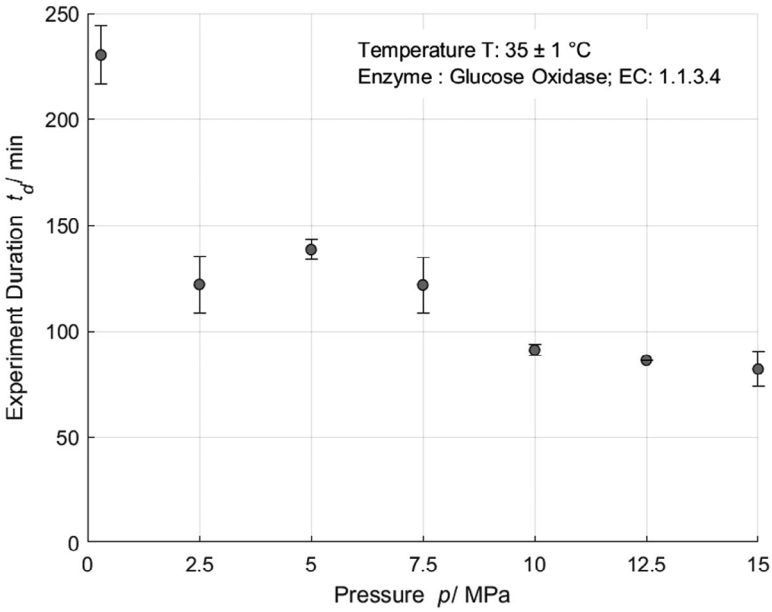

Figure 9. Dependence of the reaction time t_d on the operating pressure p. Reaction conditions: $T = 35$ °C, filling volume: 170 mL, 100 mM d-glucose substrate in sodium acetate buffer (100 mM, pH 5.4), enzyme loading of glucose oxidase: 2.9 $mg_e\ g_{carrier}^{-1}$, $\dot{V}_l$: 80 mL min^{-1}, $\dot{V}_g$: 300 $mL_N\ min^{-1}$.

The glucose conversion over time supports the hypothesis derived from the oxygen measurement. In Fig. 10, it is evident that pressure significantly impacts the initial reaction rate and the time to reach a specific conversion. Under the described conditions, the initial reaction rate of glucose oxidase increases by a factor of 4.3 between 0.3 and 10.0 MPa, and by a factor of 1.7 between 10.0 and 15.0 MPa.

5 Conclusion

This paper introduces an aerated high-pressure bioreactor. Within the scope of the paper, the hydrodynamics and the reaction rate of glucose oxidase were analyzed in the pressurized reactor. As part of the hydrodynamic investigation, parameters such as the Sauter mean diameter, gas hold-up, and resulting mass transfer area were investigated. Batch experiments with glucose oxidase were carried out to show the impact of pressure on the reaction rate. The batch experiments demonstrate that increasing the pressure, which enhances the saturation concentration and thereby the availability of oxygen, significantly reduces the reaction time from approximately 270 min to just under 90 min. Optical oxygen sensors were used with which the course of the reaction could be monitored in a time-resolved manner based on the oxygen concentration. The combined kinetic and hydrodynamic analysis revealed a bottleneck in oxygen provision by the aeration unit. Although higher pressure increases maximum oxygen solubility, the mass transfer area decreases from

 © 2024 The Author(s). Chemical Engineering & Technology published by Wiley-VCH GmbH

15214125, 0, Downloaded from https://onlinelibrary.wiley.com/doi/10.1002/ceat.202400043 by Technische Universität Hamburg Universitätsbibliothek, Wiley Online Library on [10/12/2024]. See the Terms and Conditions (https://onlinelibrary.wiley.com/terms-and-conditions) on Wiley Online Library for rules of use; OA articles are governed by the applicable Creative Commons License

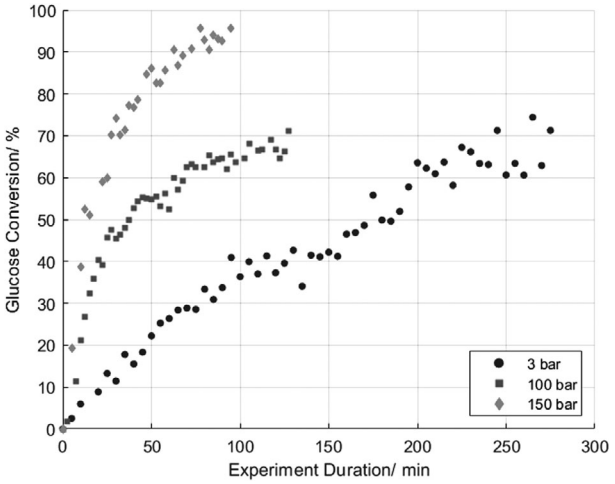

Figure 10. Conversion of glucose over time at 0.3, 10.0, and 15.0 MPa. Reaction Conditions: $T = 35$ °C, filling volume: 170 mL, 100 mM d-glucose substrate in sodium acetate buffer (100 mM, pH 5.4), enzyme loading of glucose oxidase: 2.9 $mg_e\ g_{carrier}^{-1}$, $\dot{V}_l$: 80 mL min^{-1}, $\dot{V}_g$: 300 $mL_N\ min^{-1}$.

25.0 to 1.5 m^2/m^3 at a constant air mass flow rate. This finding underscores the need for optimizing the aeration unit to improve oxygen transfer efficiency in high-pressure bioreactors.

Acknowledgments

We are grateful for the financial support provided by the Federal Ministry of Education and Research (BMBF; Grant number 031B0405A). In particular, we would like to thank our student Hani Ahmadi for his support in carrying out the elaborate experiments.

Open access funding enabled and organized by Projekt DEAL.

Symbols used

a	[$m^2\ m^{-3}$]	specific surface area
A	[m^2]	surface area
d	[m]	diameter
c	[$kg\ m^{-3}$]	concentration
I	[mV]	luminescence intensity
k_l	[$m\ s^{-1}$]	mass transfer coefficient
k_Q	[$l\ mol^{-1}\ s^{-1}$]	bimolecular quenching constant
K_H	[$mol\ l^{-1}\ pa^{-1}$]	Henry solubility constant
K_{SV}	[$l\ mol^{-1}$]	Stern–Volmer constant
n	[-]	quantity
p	[Pa]	pressure
Q	[$mol\ l^{-1}$]	quencher concentration
t	[s or min]	time
T	[°C]	temperature
u	[$m\ s^{-1}$]	velocity
V	[m^3]	volume

Greek letters

ε	[$m^3\ m^{-3}$]	gas hold-up
τ	[s]	lifetime of the emissive excited state of fluorophore
φ	[°]	phase angle

Sub- and superscripts

0	unquenched state
32	Sauter diameter
*	saturated state
∞	bulk
bc	bubble column
c	capillary
e	enzyme
g	gaseous phase
l	liquid phase
im	image
N	standard volume flow
O_2	oxygen

Abbreviations

CPA	Cube Plus Association (Equation of State)
DLR	dual-lifetime referencing
HPLC	high-performance liquid chromatography
PR	Peng Robinson
SOPAT	Smart Online Particle Analysis Technology

Data Availability Statement

Data are available on request from the authors.

References

[1] R. Daniel, *Enzyme Microb. Technol.* **1996**, *19* (*1*), 74–79. DOI: https://doi.org/10.1016/0141-0229(95)00174-3
[2] M. Roca, H. Liu, B. Messer, A. Warshel, *Biochemistry* **2007**, *46* (*51*), 15076–15088. DOI: https://doi.org/10.1021/bi701732a
[3] C. Czeslik, T. Q. Luong, R. Winter, *MRS Bull.* **2017**, *42* (*10*), 738–742. DOI: https://doi.org/10.1557/mrs.2017.211
[4] M. J. Eisenmenger, J. I. Reyes-De-Corcuera, *Enzyme Microb. Technol.* **2009**, *45* (*5*), 331–347. DOI: https://doi.org/10.1016/j.enzmictec.2009.08.001
[5] M. A. Lemos, J. C. Oliveira, M. E. Hendrickx, *Food Biotechnol.* **1999**, *13* (*1*), 13–32. DOI: https://doi.org/10.1080/08905439609549959
[6] M. Noel Marie-Olive, V. Athès, D. Combes, *High Press. Res.* **2000**, *19* (*1*), 707–712. DOI: https://doi.org/10.1080/08957950008202571
[7] F. Meersmann, *Biochim. Biophys. Acta.* **2006**, *1764* (*3*), 346–354. DOI: https://doi.org/10.1016/j.bbapap.2005.11.01
[8] P. W. Bridgman, *J. Biol. Chem.* **1914**, *19*, 511–512.
[9] J. C. Cheftel, *Food Sci. Technol. Int.* **1995**, *1* (*2–3*), 75–90. DOI: https://doi.org/10.1177/108201329500100203

 © 2024 The Author(s). Chemical Engineering & Technology published by Wiley-VCH GmbH

15214125, 0, Downloaded from https://onlinelibrary.wiley.com/doi/10.1002/ceat.202400043 by Technische Universität Hamburg Universitätsbibliothek, Wiley Online Library on [10/12/2024]. See the Terms and Conditions (https://onlinelibrary.wiley.com/terms-and-conditions) on Wiley Online Library for rules of use; OA articles are governed by the applicable Creative Commons License

[10] L. Ludikhuyze, A. Van Loey, Indrawati, C. Smout, M. Hendrickx, *Crit. Rev. Food Sci. Nutr.* **2003**, *43* (*5*), 527–586. DOI: https://doi.org/10.1080/10408690390246350

[11] V. V. Mozhaev, E. V. Kudryashova, N. Bec, *Biotechnol. Prog.* **1996**, *13*, 221–226. DOI: https://doi.org/10.1016/S0921-0423(06)80039-0

[12] B. R. de Castro Leite, A. A. L. Tribst, *Effect of High-Pressure Technologies on Enzymes*, Elsevier, Amsterdam **2023**. DOI: https://doi.org/10.1016/C2021-0-01055-5

[13] J. A. Reich, M. Aßmann, K. Hölting, P. Bubenheim, J. Kuballa, A. Liese, *J. Org. Chem.* **2022**, *18*, 567–579. DOI: https://doi.org/10.3762/bjoc.18.59

[14] M. Berheide, S. Peper, S. Kara, W. Sing Long, S. Schenkel, M. Pohl, B. Niemeyer, A. Liese, *Biotechnol. Bioeng.* **2010**, *106* (*1*), 18–26. DOI: https://doi.org/10.1002/bit.22650

[15] M. R. Chapman, S. C. Cosgrove, N. J. Turner, N. Kapur, A. J. Blacker, *Angew. Chem., Int. Ed.* **2018**, *57* (*33*), 10535–10539. DOI: https://doi.org/10.1002/anie.201803675

[16] W. K. Lewis, W. G. Whitman, *Ind. Eng. Chem. Res.* **1924**, *16* (*12*), 1215–1220. DOI: https://doi.org/10.1021/ie50180a002

[17] P. M. Wilkinson, H. Haringa, L. L. Van Dierendonck, *Chem. Eng. Sci.* **1994**, *49* (*9*), 1417–1427. DOI: https://doi.org/10.1016/0009-2509(93)E0022-5

[18] J. M. Bolivar, A. Mannsberger, M. S. Thomsen, G. Tekautz, B. Nidetzky, *Biotechnol. Bioeng.* **2019**, *116*, 503–514. DOI: https://doi.org/10.1002/bit.26886

[19] J. Jaspe, S. J. Hagen, *Biophys. J.* **2006**, *91* (*9*), 3415–3424. DOI: https://doi.org/10.1529/biophysj.106.089367

[20] C. R. Thomas, D. Geer, *Biotechnol. Lett.* **2011**, *33* (*3*), 443–456. DOI: https://doi.org/10.1007/s10529-010-0469-4

[21] P. A. Wierenga, M. R. Egmond, A. G. J. Voragen, H. H. J. De Jongh, *J. Colloid Interface Sci.* **2006**, *299* (*2*), 850–857. DOI: https://doi.org/10.1016/j.jcis.2006.03.016

[22] P. Rollbusch, M. Bothe, M. Becker, M. Ludwig, M. Grünewald, M. Schlüter, R. Franke, *Chem. Eng. Sci.* **2015**, *126*, 660–678. DOI: https://doi.org/10.1016/j.ces.2014.11.061

[23] C. Boniello, T. Mayr, *BMC Biotechnol.* **2012**, *12*, 11. DOI: https://doi.org/10.1186/1472-6750-12-11

[24] J. R. Albani, *Principles and Applications of Fluorescence Spectroscopy*, Blackwell Science, Oxford, **2007**.

[25] Y. Wei, Y. Jiao, D. An, D. Li, W. Li, Q. Wei, *Sensors* **2019**, *19* (*18*), 3995. DOI: https://doi.org/10.3390/s19183995

[26] I. Dalfen, T. Burger, C. Slugovc, S. Borisov, I. Klimant, *Sens. Actuators, B* **2022**, *352*, 131037. DOI: https://doi.org/10.1016/j.snb.2021.131037

[27] M. D. Stokes, G. N. Somero, *Limnol. Oceanogr.* **1999**, *44* (*1*), 189–195. DOI: https://doi.org/10.4319/lo.1999.44.1.0189

[28] H. C. Bittig, A. Körtzinger, C. Neill, E. van Ooijen, J. N. Plant, J. Hahn, K. S. Johnson, B. Yang, S. R. Emerson, *Front. Mar. Sci.* **2018**, *4*, 00429. DOI: https://doi.org/10.3389/fmars.2017.00429

[29] S. Hackbusch, N. Noirungsee, J. Viamonte Dominguez, X. Sun, P. Bubenheim, J. Kostka, R. Mueller, A. Liese, *Mar. Pollut. Bull.* **2020**, *150*, 110683. DOI: https://doi.org/10.1016/j.marpolbul.2019.110683

[30] A. A. L. Tribst, J. Cota, M. T. Murakami, M. Cristianini, *PLoS ONE* **2014**, *9*, e103410. DOI: https://doi.org/10.1371/journal.pone.0103410.

[31] A. Halalipour, M. R. Duff, E. E. Howell, J. Reyes-De-Corcuera, *Enzyme Microb. Technol.* **2020**, *137*, 109538. DOI: https://doi.org/10.1016/j.enzmictec.2020.109538

[32] Z. Perçin, L. Kursula, E. Löfgren, F. K. E. Byström, P. Bubenheim, M. Schlüter, A. Liese, *Biochem. Eng. J.* **2024**, *207*, 109333. DOI: https://doi.org/10.1016/j.bej.2024.109333

[33] B. Thomas, *Anwendung von Feinblasentechnologie in der Biokatalyse*, Ph.D. Thesis, Technische Universität Hamburg **2021**. DOI: 10.15480/882.3438

[34] S. B. Bankar, M. V. Bule, R. S. Singhal, L. Ananthanarayan, *Biotechnol. Adv.* **2009**, *27* (*4*), 489–501. DOI: https://doi.org/10.1016/j.biotechadv.2009.04.003

[35] G. Ozylmaz, S. S. Tukel, O. Alptekin, *J. Mol. Catal. B Enzym.* **2005**, *35* (*4–6*), 154–160. DOI: https://doi.org/10.1016/j.molcatb.2005.07.001

[36] C. Leonard, J. H. Ferrasse, O. Boutin, S. Lefevre, A. Viand, *Chem. Eng. Res. Des.* **2015**, *100*, 391–421. DOI: https://doi.org/10.1016/j.cherd.2015.05.013

[37] T. J. Lin, K. Tsuchiya, L. S. Fan, *AIChE J.* **1998**, *44* (*3*), 545–560. DOI: https://doi.org/10.1002/aic.690440306

[38] L. Han, M. H. Al-Dahhan, *Chem. Eng. Sci.* **2007**, *62* (*1–2*), 131–139. DOI: https://doi.org/10.1016/j.ces.2006.08.010

 © 2024 The Author(s). Chemical Engineering & Technology published by Wiley-VCH GmbH

15214125, 0, Downloaded from https://onlinelibrary.wiley.com/doi/10.1002/ceat.202400043 by Technische Universität Hamburg Universitätsbibliothek, Wiley Online Library on [10/12/2024]. See the Terms and Conditions (https://onlinelibrary.wiley.com/terms-and-conditions) on Wiley Online Library for rules of use; OA articles are governed by the applicable Creative Commons License